Chapter 5:

Probing the Mechanism of cpSRP43-Mediated Protein Disaggregation.

Abstract

Clearing protein aggregates is a daunting task for cells. Thus far, the best characterized "disaggregase" systems belong to the Clp/Hsp100 family of AAA+ ATPases, which use mechanical forces powered by ATP hydrolysis to remodel protein aggregates. Recently, we described an alternative system that can disassemble protein aggregates: the 43-kDa subunit of chloroplast Signal Recognition Particle (cpSRP43). With no co-chaperones or ATPase activity, cpSRP43 utilizes specific binding energy established with its substrate, light-harvesting chlorophyll a/b-binding proteins (LHCP), to power disaggregation. The molecular mechanism of cpSRP43-mediated disaggregation remains to be elucidated. In this chapter, molecular genetics analysis showed that the mechanism of disaggregation by cpSRP43 can be dissected into two steps with distinct molecular requirements: (i) initial recognition, which depends on the binding of cpSRP43 to important recognition motifs exposed on the surface of the aggregate; and (ii) subsequent remodeling/solubilization of the aggregate, which the binding interaction of LHCP to cpSRP43 competes with the internal packing interactions within the aggregate. This work establishes a useful framework to understand the mechanism of action of ATP-independent protein disaggregases.

Introduction

Protein homeostasis is vital to all cells and requires the balance of protein production, folding, localization, assembly, and degradation (*1*). Crucial to the maintenance of protein homeostasis is an elaborate network of "molecular chaperones" (*2–4*), which ensure proper protein folding and prevent protein aggregation by interacting with exposed hydrophobic residues or unstructured backbone regions that are present in non-native proteins (*2*). However, due to environmental stress, the capacity of the chaperone network could be exceeded or impaired, and protein aggregation ensues. To overcome this, cells have evolved a special set of machineries called disaggregases to rescue these protein aggregates. The most studied disaggregases belong to the Clp/Hsp100 family: yeast heat shock protein 104 (Hsp104) and its bacterial homologue ClpB (*5*). Both are members of the ATPases associated with various cellular activities (AAA+) superfamily and assemble into hexameric ring structures (*5*). These disaggregases use repetitive ATPase cycles and, in collaboration with their co-chaperones, mostly Hsp70 and Hsp40, remodel large protein aggregates via unfolding and translocation of the substrate polypeptides through their central pores (*6–8*). Although present in plant and eukaryotic mitochondria, homologues of these disaggregases have not been found in higher eukaryotes (*5*). Instead, the recent discovery of ATP-independent disaggregase activities in homogenates derived from *C. elegans* and human tissue raised the possibility that alternative disaggregation mechanisms exist in higher eukaryotes (*9, 10*).

Recently, we described a novel disaggregase system that operates independently of ATP: the 43-kDa subunit of the chloroplast Signal Recognition Particle (cpSRP43)

(*11*). The substrates for this chaperone belong to the light-harvesting chlorophyll *a/b*-binding (LHC) family of proteins, which are delivered by the cpSRP from the chloroplast stroma to the thylakoid membrane (*12*). The most abundant member of this protein family, LHCP, comprises up to 50% of the protein content in the thylakoid membrane (*13*). LHC proteins contain three highly hydrophobic transmembrane (TM) helices, making them highly prone to aggregation while traversing aqueous compartments in the cell (*13, 14*). Work from our and other laboratories have shown that cpSRP, in particular the cpSRP43 subunit, acts as a potent molecular chaperone for the LHC proteins (*11*). Intriguingly, cpSRP43 could also efficiently reverse the aggregation of its substrate proteins without the requirements for ATP hydrolysis or co-chaperones. Instead, cpSRP43 utilizes its specific binding energy to power its disaggregation activity. The basis for binding specificity is provided by a highly conserved recognition element, L18, a relatively hydrophilic 18-amino acid loop between TM2 and TM3 of the LHC proteins (*15, 16*). Nevertheless, the binding energy provided by L18 is moderate, with a dissociation constant (Kd) of ~ 1–2 μM for cpSRP43 (*17*), whereas the binding affinity between cpSRP43 and full-length LHCP is 138 nM (*11*). Moreover, the ability of cpSRP43 to prevent LHCP from aggregation implicitly indicates sequestration of hydrophobic regions of LHCP upon binding to cpSRP43. Therefore, we proposed that additional interactions must between LHCP and cpSRP43. This is supported by the fact that cpSRP43 is an elongated molecule replete with domains and motifs typically involved in protein–protein interactions: four ankyrin repeats (Ank1–Ank4) and three chromodomains (CDs) (*11, 17–20*). These domains can provide possible interaction interfaces for the LHCP molecule.

cpSRP43 represents an example of a novel class of disaggregases that operate with energy derived entirely from binding interactions with its substrates. Understanding its mechanism will provide valuable insights into alternative approaches that the cells use to handle protein aggregates. Previous kinetic analyses revealed that disaggregation is a cooperative process and suggested that cpSRP43 binds to and actively remodels the LHCP aggregate (*11*). We propose that initial recognition of the LHCP aggregate occurs via interactions with L18. This is substantiated by evidence from both electron paramagnetic resonance (EPR) and chemical modification experiments (V.Q. Lam and T.X. Nguyen, unpublished results), both of which showed that LHCP aggregates form by burying their hydrophobic TM segments in the interior, whereas the L18 motif is exposed on the exterior, corroborating an earlier speculation that LHCP aggregates are micellar (see Chapter 4). These results suggest an attractive starting point for disaggregation: the LHCP aggregates expose the L18 motif on the exterior, poised for recognition by cpSRP43.

After initial recognition of the aggregate, what happens next? The observed cooperativity suggested that binding of one cpSRP43 facilitates binding of subsequent cpSRP43 molecules, implying an aggregate remodeling step after cpSRP43 binding. This step could be independent of binding to the exposed L18. Using distinct classes of mutants, we present evidence that (i) the remodeling step could be distinguished from the initial binding step and (ii) the stabilities of both the starting LHCP aggregates and the final cpSRP43•LHCP soluble complex play large roles in determining the extent of aggregate remodeling and re-solubilization.

Materials and Methods

Materials. To construct the LHCP TM mutant proteins, the expression plasmid encoding LHCP was modified to contain a pair of unique restriction sites before and after the regions coding TM1, TM2, or TM3. Then, the sequences coding for original TMs were replaced with PCR fragments encoding exogenous TMs using corresponding restriction sites. TM deletion mutants were constructed using QuikChange (Stratagene) with primers omitting the coding regions of TM1, TM2, or TM3. Description of each mutant was summarized in Supplementary Table 5.S1. Lhcb5 cystein mutants were constructed using QuikChange (Stratagene). LHCP and its variants were purified under a denaturing condition as described (*11*).

Light scattering. Light scattering experiments were performed as previously described (*11*). To determine K_d^{app} by light scattering, prevention of LHCP aggregation was used. Briefly, absorbance at 360 nm was measured after 10 minute incubation with varying concentrations of cpSRP43. The light scattering signals were normalized to the absorbance recorded from the sample with no chaperone, and percentage soluble (% soluble) was calculated by subtracting percentage light scattering at each cpSRP43 concentration from 100. The light scattering is linearly proportional to the concentration of LHCP except at very low concentrations. Data were fit with the quadratic eq 1

$$\%\ \text{soluble} = 100 \times \frac{[\text{LHCP}] + [\text{cpSRP43}] + K_d^{app} - \sqrt{([\text{LHCP}] + [\text{cpSRP43}] + K_d^{app})^2 - 4 \times [\text{LHCP}][\text{cpSRP43}]}}{2 \times [\text{LHCP}]} \quad \textbf{(1)}$$

in which K_d^{app} is the apparent dissociation constant. Due to the inaccuracy of the measurement at very low unbound LHCP concentrations (see Chapter 4), the K_d^{app} values could be mildly underestimated. Nevertheless, comparison of the K_d values measured by

light scattering and fluorescence anisotropy for wild-type LHCP (111±3 nM compared to 138 nM measured by anisotropy; (*11*)) and a few of the LHCP TM mutants showed that the two methods produced comparable numbers (Supplementary Figure 5.S1).

Disaggregation reactions were performed as previously described (*11*), with the exception that the aggregation period was 1 minute. The disaggregation time courses were fit to an exponential function (eq 2)

$$A = A_f + \Delta A e^{-k_{obsd} t} \qquad (\mathbf{2})$$

in which A is the observed light scattering, A_f is the amount of light scattering at $t \rightarrow \infty$, ΔA is the extent of light scattering change, and k_{obsd} is the observed rate constant. The observed light scattering is normalized to that prior to the addition of cpSRP43 for each disaggregation reaction. The fractions disaggregated (θ) were calculated by subtracting A_f from 1. The concentration dependences of fractions disaggregated were fit to eq 3

$$\theta = \theta_{\max} \times \frac{[\text{cpSRP43}]^n}{(K_m^{dis})^n + [\text{cpSRP43}]^n} \qquad (\mathbf{3})$$

in which θ_{max} is the extent of disaggregation at saturating cpSRP43 concentration, K_m^{dis} is the average affinity of cpSRP43 to LHCP aggregates, and n is the Hill coefficient.

Kinetic analysis was performed and analyzed as described previously (*11*). Briefly, the concentration dependence of the disaggregation rate constants, k_f, was fit to eq 4,

$$k_f = k_0 \times \frac{K_d^n}{K_d^n + [\text{cpSRP43}]^n} + k_{\max} \times \frac{[\text{cpSRP43}]^n}{K_d^n + [\text{cpSRP43}]^n} \qquad (\mathbf{4})$$

in which k_0 is the rate of spontaneous LHCP disaggregation in the absence of the chaperone, K_d is an average equilibrium dissociation constant for binding of cpSRP43 to LHCP aggregates, n is the Hill coefficient, and k_{max} is the disaggregation rate constant at saturating cpSRP43 concentration.

Fluoresecence anisotropy. Fluorescence labeling of LHCP and its variants and fluorescence anisotropy were carried out as described previously (*11*).

Sedimentation assay. Urea solubilization experiments and data analyses were carried out as described (Chapter 4). Briefly, re-solubilization of the LHCP aggregates by urea was monitored by SDS-PAGE. The intensity of the Coomassie-stained bands for the pellet and soluble fractions were quantified using ImageJ (*21*). The data were fit with a function derived from the two-state model for protein folding (*22*), shown below:

$$\theta = \frac{1}{1 + e^{-m(U_{50} + [urea])/RT}} \qquad \textbf{(5)}$$

where θ is the fraction soluble [s/(s+p)], R is the gas constant, and T is temperature. The fit gave U_{50}, which is the urea concentration at which 50% of LHCP aggregate was solublized, and m, which represents a constant of proportionality. ΔG^o, which represents free energy of transfer of the aggregate from water to urea, could be calculated from fits to eq 5 (= $-mU_{50}$).

Mathematical analyses. All correlations were obtained by regression fits of the obtained parameters in Table 5.3 using the "polyfitn" tool in Matlab (*23*).

Results

The current working model of LHCP disaggregation by cpSRP43 involves two steps: (i) initial binding and (ii) subsequent remodeling of the aggregate. To provide supporting evidence for this model, we sought mutants that specifically block distinct stages of disaggregation. In this work, we present thermodynamic and kinetic analyses of disaggregation reactions of aggregates formed by various LHCP mutants and characterize intrinsic properties of these mutants to reveal the distinct molecular requirements for each step of disaggregation. Table 5.1 summarizes the parameters used for comparison in this study.

Binding to L18 on the LHCP aggregate is the first step to disaggregation.

Previous results led us to propose that cpSRP43 recognizes and binds to the LHCP aggregates via interactions with the solvent-exposed L18 motif (T.X. Nguyen and V.Q. Lam, unpublished results). If this were the case, mutants of LHCP or cpSRP43 that specifically impair the L18–cpSRP43 interaction would exhibit defects in the disaggregation at low chaperone concentrations. However, as binding is a higher-order process, the defects of these mutants should be rescued when a sufficiently high concentration of the chaperone is used to drive binding. To test this hypothesis, we examined the disaggregation efficiencies of the L18 mutants on LHCP or the L18-binding mutants on cpSRP43.

The crystal structure of the cpSRP43–L18 complex identifies Arg161 in the ankyrin repeats of cpSRP43 as an important hydrogen bond partner with the L18 peptide (*17*). As expected, the cpSRP43-R161A mutant significantly reduces its binding affinity

to solubilized LHCP (K_d = 1.2 μM, compared to 138 nM for wild-type cpSRP43; Table 5.2; (*11*)). Reciprocally, we identified two mutants in the L18 region of Lhcb5, a close homologue of LHCP, that were defective in binding to cpSRP43: H160C and L170C. Using the light scattering assay for prevention of aggregation, we could conveniently measure apparent binding affinity of various LHC protein mutants (see Methods). The concentration dependence of the amount of the soluble LHCP gave a binding curve that could be fit with a quadratic equation to yield an apparent dissociation constant (K_d^{app}), which is comparable to those measured by fluorescence anisotropy (See Methods and Supplementary Figure 5.S1; (*11*)). This assay yields K_d^{app} values of 30 nM and 1.1 μM for Lhcb5-H160C and -L170C, respectively, compared to 10 nM for wild-type Lhcb5 (Table 5.2 and Supplementary Figure 5.S2).

Consistent with a defect in recognition of the LHCP aggregate, 10 μM of cpSRP43-R161A could not reverse LHCP aggregation (Figure 5.1A, magenta), whereas almost 100% reversal of aggregation could be obtained for wild-type cpSRP43 at this concentration (Figure 5.1A, black; (*11*)). However, when the concentration of the mutant chaperone was raised to compensate for the binding defect, cpSRP43-R161A could efficiently reverse LHCP aggregation (Figure 5.1B, magenta, and Table 5.2). Analogously, the aggregates formed by the L18 mutants in Lhcb5 showed defects in the disaggregation reaction that can be rescued by higher cpSRP43 concentrations (Figure 5.1B and Table 5.2). The more severe mutant, Lhcb5-L170C, required a much higher concentration of cpSRP43 to achieve efficient solubilization of the aggregate than the less severe mutant (Figure 5.1B, red). Together, the results in this section showed that L18 binding is an important requirement for disaggregation, and suggest that this initial

recognition step can be uncoupled from the subsequent step(s) that are unimolecular in nature.

cpSRP43 makes non-specific contacts with the hydrophobic TM segments.

In order to remodel the aggregate in the subsequent step(s), cpSRP43 must compete with the internal packing of the aggregates and provide alternative binding interactions for the hydrophobic TMs that were buried inside the aggregate. However, it was unclear whether these interactions are highly sequence-specific, like that of the L18, or are more generic hydrophobic contacts, like those of other promiscuous chaperone–substrate interactions (*2*). To address this question, we constructed various LHCP mutants in which the individual TMs are deleted or replaced with other TM segments in LHCP or the TMs from unrelated membrane proteins (see Supplementary Table 5.S1 for nomenclature and description of all LHCP TM mutants used in this study). We reasoned that if these interactions were sequence-specific, deletion or replacement of the TM helices should result in significant reduction in cpSRP43's chaperone activity, analogous to mutations in the L18 motif (*11*). On the other hand, if these interactions arose from generic hydrophobic interactions or backbone contacts, many of these TM replacements would not result in deleterious defects in the chaperone activity.

We purified several LHCP TM mutants and showed that cpSRP43 could still bind and protect them from aggregation (Figure 5.2, A and B). Deletion of TM helices did not result in significant defects in the chaperone activity of cpSRP43, although these LHCP deletion mutants still aggregated to similar extents as wild-type LHCP (Figure 5.2 and data not shown). Some mutants, such as ΔTM3, SERP2, Sec2, interact even better and

are hence more readily protected by cpSRP43, whereas other mutants, such as 1-3-2, 1-2-2, and 1-1-3 exhibited moderately lower (two–fivefold) affinity to cpSRP43 (Figure 5.2B). Nevertheless, virtually all of the TM replacement mutants exhibit moderate-to-high binding affinities for cpSRP43 in their soluble form, and these binding affinities are significantly higher than that of cpSRP43 for the isolated L18 peptide (*17*). This strongly suggests that the hydrophobic TMs in LHCP contribute additional binding interactions with cpSRP43, and these interactions are fairly generic and highly adaptable, in contrast to the strictly sequence-specific interactions of cpSRP43 with the L18 motif. Finally, these results show that cpSRP43 can protect a variety of aggregation-prone proteins, as long as the L18 motif is present to provide specific recognition.

Some LHCP TM mutant aggregates are virtually irreversible.

Since these TM mutants contain identical L18 motifs, they provide a good collection of substrates to probe for other molecular requirements for efficient disaggregation. Using the established light scattering assay (Supplementary Figure 5.S3), we analyzed both the equilibrium and the rate of the disaggregation reactions for these LHCP TM variants. As a group, they exhibited striking differences in both thermodynamics and kinetics of disaggregation (Figure 5.3 and Table 5.3).

Plots of the disaggregated fraction showed cooperative dependence on the concentrations of cpSRP43 (Figure 5.3A). Fits of these plots gave two important thermodynamic parameters: (i) the average affinities of cpSRP43 for binding to the various LHCP aggregates (K_m^{dis}), which reflect the concentrations of cpSRP43 needed for efficient disaggregation; and (ii) the disaggregated fractions at saturating cpSRP43

concentration (θ_{max}), which represent the extent of disaggregation reactions for these LHCP mutant aggregates once cpSRP43 has bound to the aggregate. Additionally, the $\theta_{4\,\mu M}^{app}$ values, the extent of disaggregation at sub-saturating cpSRP43 concentration, provide important practical measures of disaggregation efficiency especially for mutants whose θ_{max} values cannot be accurately determined.

Surprisingly, even though these LHCP TM mutants showed significant binding interactions with cpSRP43 in their soluble forms, we found that some LHCP TM mutants, especially 1-1-3, ΔTM2, 1-2-2, and 1-3-2, were virtually irreversible (Figure 5.3A, red, and Supplementary Figures 5.S4–5.S6). To a lesser extent, ΔTM1 and 1-2-1 also show large defects in disaggregation equilibrium (Supplementary Figures 5.S7 and 5.S8). These mutants carry solvent-exposed wild-type L18 in their aggregates (T.X. Nguyen, unpublished results). Therefore, we hypothesized that this group of mutants did not block the recognition step but possibly disrupted the remodeling step. On the other hand, some TM mutants showed disaggregation efficiencies that are similar or even better than the wild-type LHCP aggregate (Figure 5.3, blue and green, and Supplementary Figures 5.S9–5.S12).

The disaggregation rate constants also showed cooperative dependence on the concentrations of cpSRP43 (Figure 5.3B). The k_{max} values, which represent the disaggregation rate constants at saturating cpSRP43 concentrations, reveal significant differences in disaggregation kinetics among these LHCP TM mutants (Table 5.3). The irreversible mutants, if at all, were disaggregated at extremely slow rates (Figure 5.3B, red, and Supplementary Figures 5.S4–5.S6). Meanwhile, other mutant aggregates, notably those of ΔTM3, SERP2, Sec2, and Cyb2, could be re-dissolved more easily than

the wild-type aggregate and exhibited much faster disaggregation rates (Figure 5.3 A and B, green, and Supplementary Figures 5.S10–5.S12).

Overall, the results in this section indicated that (i) the irreversible mutants specifically block the remodeling step with minimal perturbations in binding, providing additional support for the two-step disaggregation mechanism, and (ii) this group of LHCP TM mutants displays a wide range of disaggregation efficiencies and kinetics (Table 5.3). Further analyses of the molecular features underlying these differences may provide valuable insights into the molecular mechanism of protein disaggregation.

The irreversible LHCP TM mutants form ultra-stable aggregates.

Unlike the L18-binding mutants, the irreversible LHCP TM mutants bind reasonably well to cpSRP43. What then could cause the drastic defects in the equilibrium and kinetics of disaggregation? Previous results from chemical modification and EPR experiments showed that the TM helices engage in strong interactions and are buried inside the aggregate (T.X. Nguyen and V.Q. Lam, unpublished results). Since the TM helices are considerably altered in these LHCP mutants, we hypothesized that the internal packing interactions of their aggregates are different and may play a role in disaggregation. To test this hypothesis, we probed the strength of the packing interactions inside the aggregates using urea solubilization (Chapter 4). For comparison, we used the U_{50} values, the urea concentrations at which 50% of LHCP aggregates are solubilized (Table 5.1), which provide empirical measures for the strength of the packing interactions that stabilize the aggregates formed by the LHCP TM variants.

As expected, aggregates from LHCP TM mutants exhibited a wide range of stabilities, with the U_{50} values from 2.5 to 5.7 M (Table 5.3). Mutant aggregates that are easily disaggregated collectively displayed low U_{50} values (2.5–3.6 M; Figure 5.4, green, and Supplementary Figures 5.S10–5.S12), whereas wild-type LHCP and the neutral mutants exhibited intermediate U_{50} values (3.7–4.7 M; Figure 5.4, black and blue, and Supplementary Figures 5.S7–5.S9). Importantly, the four irreversible mutants that could bind but were extremely slow and inefficient in disaggregation had the highest U_{50} values (4.7–5.7 M; Figure 5.4, red, and Supplementary Figures 5.S4–5.S6). These results indicate that the internal packing interactions are crucial in determining the extent of a disaggregation reaction.

Molecular determinants of disaggregation efficiency.

To understand the contributions of the molecular features dictating the disaggregation more rigorously, we correlated the extent of disaggregation with the two thermodynamic parameters that we measured, the K_d^{app} values and the U_{50} values. First, we reasoned that binding between cpSRP43 and the LHCP monomer should provide the ultimate driving force for the disaggregation reaction, as the cpSRP43•LHCP soluble complex is the product of the reaction. However, we barely observed a correlation between the apparent binding affinities of these mutants in their soluble forms (K_d^{app}) with the extent of disaggregation ($\theta_{4\,\mu M}^{app}$) (Figure 5.5A; $R^2 = 0.58$).

A qualitative observation that the four irreversible mutants did not have severe binding defects yet were very difficult to reverse (Table 5.3, red) prompted us to ask if other properties, especially the internal packing interactions, additionally contributed to

the disaggregation efficiency. When we included a dimension representing the stability of the LHCP aggregates in our mathematical analysis, we could observe an improvement in the correlation between the extent of disaggregation and the stabilities of both the final product (the cpSRP•LHCP soluble complex; K_d^{app}) and the starting aggregate (U_{50}) (Figure 5.5B; $R^2 = 0.77$). The data points highlighted in blue in Figure 5.5 were derived from the set of Lhcb5 proteins (Figure 5.1B), which aggregated more slowly and presented another layer of complication for disaggregation analysis compared to the set of LHCP TM mutants. It is possible that these different LHC proteins were disaggregated in pathway-specific manners and that they had additional less well-understood molecular requirements for efficient disaggregation. Presently, we could not unambiguously pinpoint the origins of these outliers. Nevertheless, these correlational analyses show that both binding to LHCP and competing with aggregate packing interactions are crucial in determining the overall disaggregation efficiencies.

Kinetic analysis provides additional insights into the rate-limiting step of the mechanism. We observed a decent negative correlation between the U_{50} values and the maximal disaggregation rate constants, k_{max} (Figure 5.6A; $R^2 = 0.78$). This observation strongly suggests that packing interactions inside the aggregates determine the activation barrier that cpSRP43 has to overcome during disaggregation. Further analyses of the differences in the equilibrium and the rates of disaggregation between the wild-type and mutant LHCPs yielded valuable information regarding the transition state of the disaggregation reaction. For each mutant, we calculated its perturbation on the free energy of the overall reaction ($\Delta\Delta G \sim \ln K^{app}$) relative to its perturbation on the free energy of the transition state ($\Delta\Delta G^{\ddagger} \sim \ln k^{app}$) and observed a linear relationship between

the two terms for the set of the LHCP mutants (Figure 5.6B). Analogous to the classical Bronsted β-value analysis or the Φ-value analysis of the protein-folding mutants (*22*), this correlation could be used to infer information about the transition state of the reaction. The fractional slope of 0.5 (Figure 5.6B) could not be unambiguously interpreted. It possibly resulted from either the partially formed cpSRP43–LHCP interactions or the mixture of transition states from different kinetic pathways (*22*). However, the value significantly higher than zero implies that, in the transition state of the reaction, interactions between LHCP molecules and the disaggregase were already formed, albeit not as strong as those ultimately present in the final soluble product.

Discussion

Thermodynamic and kinetic analyses of the disaggregation reactions of various LHCP mutants allow us to dissect the molecular steps during the disassembly of the LHCP aggregates by cpSRP43, and revealed several distinct and crucial molecular requirements for the disaggregation reaction mediated by cpSRP43. These data led us to propose a two-step working model for the action of cpSRP43 as a protein disaggregase (Figure 5.7A).

Step 1: Binding to the LHCP aggregate.

To initiate the disaggregation reaction, cpSRP43 must recognize and engage the LHCP aggregates. This likely occurs via cpSRP43's binding to its primary recognition motif L18, which is presented on the exterior of the LHCP aggregate (Figure 5.7A, step 1). In support of this model, mutants of cpSRP43 or LHC proteins that disrupt the interactions between the L18 motif and cpSRP43 specifically affect this initial step mainly by destabilizing the intermediate cpSRP43•$LHCP_{agg}$ complex due to their compromised affinity of the L18 motif (Figure 5.7B, magenta line). This increases the free energy cost for the first binding step (Figure 5.7B, ΔG_{bind} magenta vs. black). As binding is a higher-order process, this defect could be overcome by increasing the concentration of the disaggregase.

Markedly, there is a positive correlation between the overall apparent binding affinities between cpSRP43 and soluble LHCP (K_d^{app}) and the binding affinities between cpSRP43 and LHCP aggregates (K_m^{dis}) (Table 5.3). This is surprising because, if the aggregate recognition step involved exclusively the interactions between the L18 motif

and cpSRP43, the K_m^{dis} values should reflect only the affinity of cpSRP43 to the L18 motif and should be almost invariant for the group of LHCP TM mutants carrying wild-type L18 motifs. The strong correlation could imply that more than, in the recognition step, cpSRP43 also interacts with other regions in LHCP besides L18. In support of this speculation, recent study has proposed that cpSRP43 makes additional contacts with LCHP, particularly the beginning of the third TM helix of LHCP (*24*). Alternatively, this correlation could suggest different presentations of the L18 motifs by the aggregates formed by various LHCP TM mutants such that the average binding constants to the aggregates are different. Further studies to distinguish these possibilities are needed.

Step 2: Remodeling of the LHCP aggregate.

For the subsequent aggregate remodeling step, cpSRP43 must break the aggregate packing interactions and provide sufficient binding surfaces for the dislodged LHCP monomers, preventing re-aggregation (Figure 5.7A, step 2). Once cpSRP43 is bound to the aggregate, the extent of the disaggregation reaction (represented by θ_{max}) is determined by the free energy of the remodeling step, which is the difference in free energy between the cpSRP43•LHCP complex and the intermediate cpSRP43•$LHCP_{agg}$ complex (Figure 5.7B, ΔG_{rem}). Therefore, the modulations in the stability of either complex will induce changes in the equilibrium of disaggregation. For example, the irreversible mutants form ultra-stable aggregates (Figure 5.4, red, and Table 5.3, red), which likely result in the stabilization of the intermediate to the same extent (Figure 5.7C). This decreases the drive for the remodeling step. For these mutants, this stabilization of the aggregate and the intermediate state could render the subsequent

remodeling step energetically unfavorable (Figure 5.7C, red vs. black ΔG_{rem}). In this scenario, disaggregation of these mutants cannot efficiently occur even at high cpSRP43 concentrations, because the remodeling step is independent of chaperone concentration. On the contrary, the mutants that are easily reversible (Table 5.3, green) have an opposite free energy landscape. Their aggregates are destabilized, and their soluble cpSRP43•LHCP complexes are stabilized compared to wildtype. Hence, they exhibit greater disaggregation efficiency due to a larger thermodynamic drive.

The stability of the LHCP aggregates also influences the disaggregation kinetics, as suggested by the observed negative correlation between the disaggregation rates and the U_{50} values (Figure 5.6A). The mutants that form less stable aggregates and are easily reversible also have lower activation barrier for remodeling, resulting in a faster disaggregation rate. In contrast, the irreversible mutants with ultra-high stability of their aggregates (Figure 5.7C, red) also have a much larger activation barrier to proceed (Figure 5.7C, red $\Delta G^{\ddagger}$) and hence exhibit slower disaggregation kinetics. The manifestation of the mutational effects on the disaggregation rate is remarkable, and strongly suggests that the rate-limiting transition state for the disaggregation process is fairly late and requires disruption of a substantial amount of internal structures within the aggregate.

Comparison with the Clp/Hsp100 family of protein remodeling complexes.

It is noteworthy to compare lessons learned from cpSRP43 to those from the force-generating protein-remodeling complexes such as the Clp/Hsp100 family of ATPases. First, how do the disaggregases select their substrates in the initial step? We

note that the two disaggregase systems differ greatly in their substrate selection. cpSRP43 is a specific chaperone for the LHC family of proteins, whereas the Clp/Hsp100 ATPases handle a large fraction of the cellular proteome (*25*). The specificity in cpSRP43-mediated disaggregation is imparted by the recognition of the strictly-conserved L18 motif on the exterior of the aggregate. On the other hand, the AAA+ remodeling machines displays much more promiscuity in substrate selection. A binding study using a peptide library showed that ClpB prefers peptides that are enriched in aromatic and basic residues with no specific sequence patterns (*26*). These peptides comprise the hydrophobic cores of most native proteins and may be exposed as disordered loops when proteins aggregate (*6*). The less stringent requirements for their substrates allow the Clp/Hsp100 ATPases to be the central disaggregases for the cells.

Second, how do these disaggregase remodel their substrates in the subsequent step(s)? Although the precise molecular details remain to be elucidated, our results herein provide some clues to the mechanism of aggregate remodeling by cpSRP43. First, the cooperativity observed in disaggregation strongly argues for the changes in the structure of the LHCP aggregates brought upon by cpSRP43 binding and suggests possible destabilization of the aggregates. Since the aggregate formation is a cooperative process, as evident in both urea solubilization and disaggregation by cpSRP43, such destabilization likely collapses the whole structure. Second, the negative correlation between the rate of disaggregation and the global stability of the aggregates (Figure 5.6A) further supports disassembly of whole aggregates (see more below). Third, after disaggregation is complete, cpSRP43 remains in soluble complexes with dislodged LHCP monomers to prevent re-aggregation, and the extent of this equilibrium is

determined by the binding affinities between the LCHP monomer and cpSRP43. In contrast, Clp/Hsp100 ATPases use the threading mechanism for protein remodeling (*6*). Cycles of ATP binding and hydrolysis govern how the residues at the central pores of these hexameric rings bind or release substrates in a unidirectional manner, forcing polypeptides through small constrictions and possibly dislodging one aggregated molecule at a time (*26, 27*). Unfortunately, the relationship between the stability of the aggregates and the disaggregation rate has not been systematically investigated. Nevertheless, lessons learned from other members of the Clp/Hsp100 ATPases, such as the protease-associated ClpA and ClpX unfoldases, can provide valuable insights. For both unfoldases, it has been shown that the overall thermodynamic stability of the native protein substrates poorly correlates with the effectiveness of unfolding/degradation (*28, 29*). Rather, the local structure and the stability of the regions adjacent to the degradation tags have a dominant effect on unfolding (*28–30*). This observation corroborates with the proposed threading mechanism for the Clp/Hsp100 family, because these remodeling machines sequentially unravel their substrates from the recognition sites. This is in stark contrast with the case of cpSRP43, in which global stability of the aggregate correlates well with the rate of disaggregation (Figure 5.6A), suggesting that the two systems utilize distinct mechanisms in remodeling the protein/aggregate substrates. Instead of remodeling sequentially in parts like the Clp/Hsp100 proteins, cpSRP43 likely works on the whole aggregate at once.

Perspective.

The observation that cpSRP43 is only found in green plants suggests possible co-evolution with its substrates, the LHC proteins. Dedicated to the LHC protein transport,

cpSRP43 can establish extensive binding interactions with its substrate, sufficient to power its disaggregase activity. By the same token, it is intriguing that LHC proteins make the L18 accessible even when they form aggregates, allowing for binding to cpSRP43. Although the physiological significance of the disaggregase activity of cpSRP43 remains to be shown, it is conceivable that this activity is beneficial for cpSRP43, as it might be able to rescue unproductive membrane targeting or insertion of its substrates (*31*).

Recent works have reported protein-based, ATP-independent disaggregation activities in eukaryotic tissues (*9, 10*). Although the molecules responsible for these activities and their mechanism have not been identified, these findings suggest that cells have evolved methods to reverse protein aggregates that are alternative to the usage of ATP hydrolysis. As our work has shown, using binding energy to replace packing interactions inside the aggregates can be an efficient strategy for disaggregation. cpSRP43 now stands as a rare example of a class of disaggregases that can remodel and re-solubilize insoluble protein aggregates using only binding energy.

Table 5.1 Description of the thermodynamic and kinetic parameter discussed in this study

Parameter	Definition	Assay	Reference[1]
$\boldsymbol{\theta_{max}}$	Maximal fraction disaggregated at saturating cpSRP43 concentration	Light scattering (Disaggregation)	**3**
$\theta_{4\,\mu M}^{app}$	Fraction disaggregated at sub-saturating cpSRP43 concentration (4 μM)	Light scattering (Disaggregation)	**3**
$\boldsymbol{K_m^{dis}}$	Average equilibrium dissociation constant for binding of cpSRP43 to LHCP aggregates	Light scattering (Disaggregation)	**3**
n	Hill coefficient	Light scattering (Disaggregation)	**3**
$\boldsymbol{k_{max}}$	Maximal disaggregation rate constant	Light scattering (Disaggregation)	**4**
$\boldsymbol{K_d^{app}}$	Apparent dissociation constant for cpSRP43•LHCP complex	Light scattering (Prevention) and fluorescence anisotropy	**1**
$\mathbf{U_{50}}$	Urea concentration for 50% re-solubilization of $LHCP_{agg}$	Sedimentation	**5**

[1]Reference to equations in Methods

Table 5.2 Summary of the thermodynamic parameters of the L18-binding mutants

Construct	K_d^{app} **(nM)**	K_m^{dis} **(μM)**	θ_{max}	$\theta_{4\,\mu M}^{app}$	$\theta_{50\,\mu M}^{app}$
cpSRP43 R161A	1200[1]	>50[2]	N.D.	0.02	0.40
Lhcb5	10	4.1	1.06	0.51	1.06
Lhcb5 H160C	30	11.4	0.85	0.12	0.79
Lhcb5 L170C	1100	>50[2]	N.D.	0.03	0.35

N.D. = not determined. Values reported are from Figure 1.
[1]previously determined by fluorescence anisotropy in (*11*)
[2]denotes the values at the highest cpSRP43 concentration used

Table 5.3 Summary of the thermodynamic and kinetic parameters of the LHCP TM mutants

Construct	θ_{max}	$\theta_{4\,\mu M}^{app}$	K_m^{dis} (μM)	n	k_{max} (s^{-1})	K_d^{app} (nM)	U_{50} (M)
WT	0.99±0.03	0.70±0.06	2.6±0.2	2.5±0.1	0.048±0.011	111±3	3.8±0.2
1-3-3	1.00±0.05	0.72±0.10	2.8±0.4	2.5±0.6	0.046±0.000	144±34	3.7±0.1
SERP3	1.05±0.06	0.30±0.01	6.0±0.7	2.3±0.3	>0.030[1]	207±51	4.0±0.1
1-2-1	0.88±0.01	0.02±0.00	12.8±0.9	3.4±0.0	0.015±0.000	234±16	4.4±0.3
ΔTM1	0.91±0.00	0.09±0.04	8.4±0.8	3.1±0.3	>0.025[1]	413±76	4.7±0.0
SERP2	1.04±0.04	0.95±0.03	1.3±0.1	2.2±0.4	0.109±0.006	9±5	3.5±0.1
ΔTM3	0.98±0.02	0.95±0.03	1.7±0.1	4.1±0.0	0.065±0.003	26±12	2.5±0.1
Sec2	1.09±0.04	0.81±0.03	2.2±0.3	1.9±0.0	0.082±0.019	36±17	3.3±0.1
Cyb2	1.04±0.05	0.69±0.00	2.9±0.2	2.1±0.0	0.055	51±24	3.6±0.2
ΔTM2	N.D.	0.01	>75[1]	N.D.	0.003	216±88	5.7±0.1
1-2-2	N.D.	0.00	>75[1]	N.D.	>0.002[1]	489±95	4.7±0.1
1-3-2	N.D.	0.03	>60[1]	N.D.	>0.004[1]	456±206	4.8±0.1
1-1-3	N.D.	0.00	>60[1]	N.D.	0.003	490±57	5.7±0.1

N.D. = not determined. Values reported are average from two or more independent experiments ± S.D.
[1]denotes the values at the highest cpSRP43 concentration used

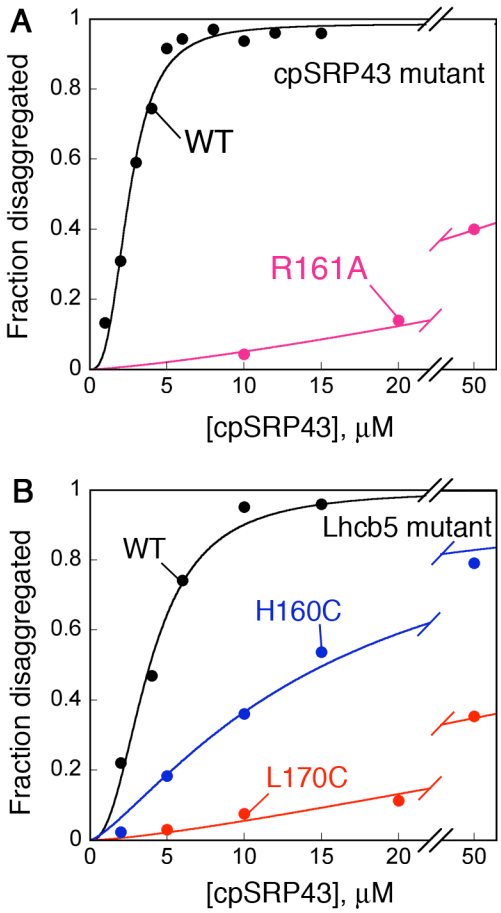

Figure 5.1 L18 mutants uncouple initial binding from subsequent aggregate solubilization. (A) Concentration dependence for disaggregation of LHCP by wild-type (black) or R161A mutant (magenta) of cpSRP43. (B) Concentration dependence for disaggregation of Lhcb5 (black), Lhcb5-H160C (blue), and Lhcb5-L170C (red) by wild-type cpSRP43.

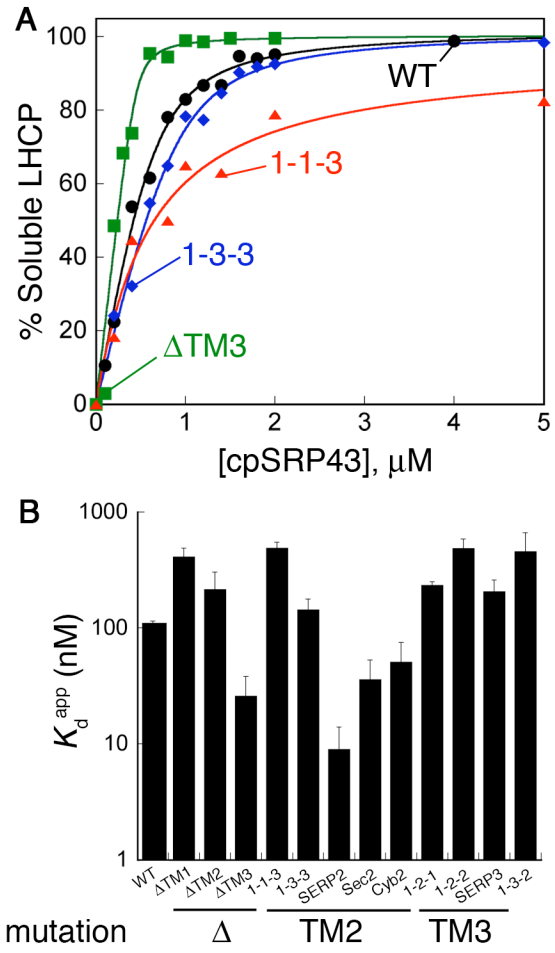

Figure 5.2 cpSRP43 can interact with LHCP TM mutants. (A) Binding of cpSRP43 to LHCP and its TM mutants as measured by light scattering. The data were fit to eq 1 and gave K_d^{app} values of 109 nM for LHCP (black), 120 nM for 1-3-3 (blue), 13 nM for ΔTM3 (green), and 529 nM for 1-1-3 (red). (B) K_d^{app} values of the LHCP TM mutants in this study. Values are from Table 5.3. See Supplementary Table 5.S1 for nomenclature and description of the LHCP TM mutants.

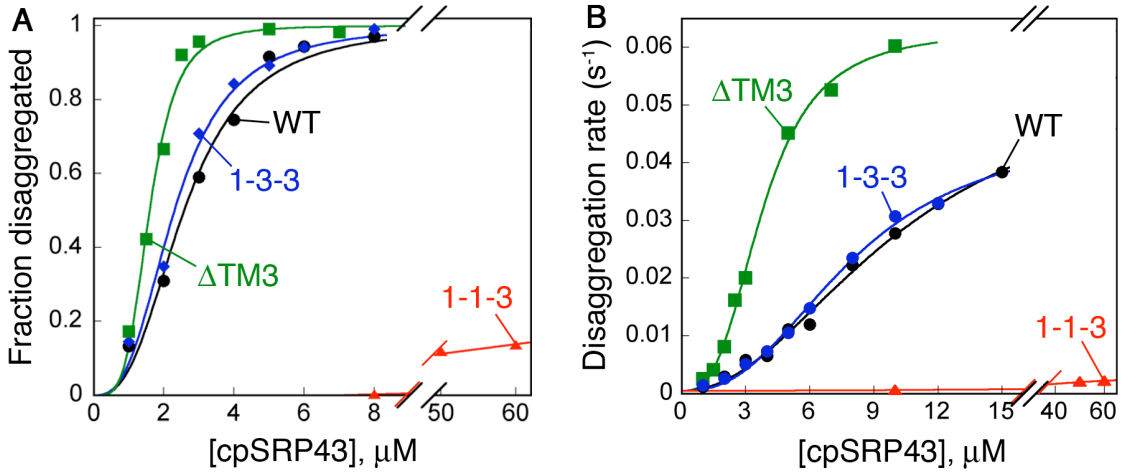

Figure 5.3 LHCP TM mutants show different disaggregation efficiencies. Concentration dependences of disaggregation equilibrium (A) and rate (B) for LHCP (black), 1-3-3 (blue), ΔTM3 (green), and 1-1-3 (red). For A, the data were fit to eq 3 and gave θ_{max}, K_m^{dis} and n values. $\theta_{4\,\mu M}^{app}$ values were also extracted from these plots. For B, the data were fit to eq 4 and gave k_{max} values. Thermodynamic and kinetic parameters were reported in Table 5.3.

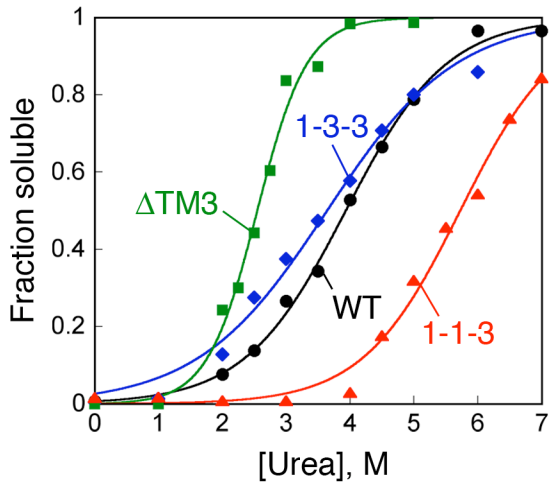

Figure 5.4 The irreversible LHCP mutant aggregates are ultra-stable. Urea solubilization curves of LHCP and its TM mutants. The data were fit to eq 5 and gave U_{50} values of 3.9 M for LHCP (black), 3.6 M for 1-3-3 (blue), 2.5 M for ΔTM3 (green), and 5.7 M for 1-1-3 (red).

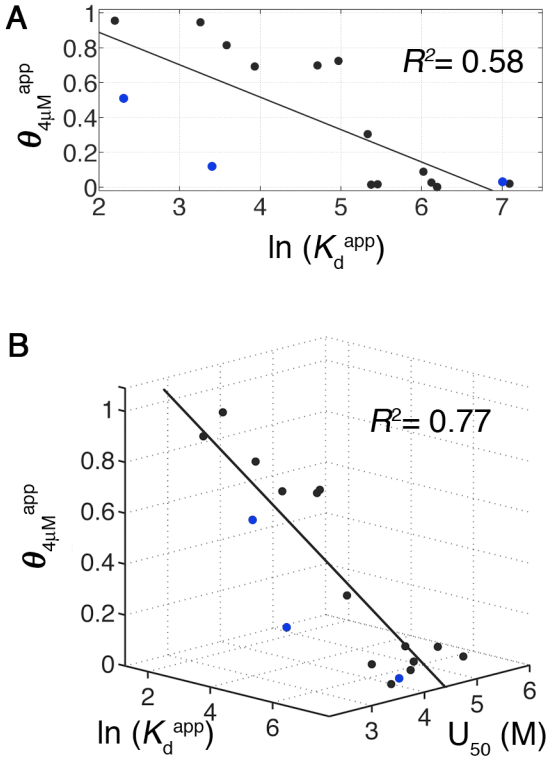

Figure 5.5 Stability of both the soluble cpSRP43•LHCP complex and the LHCP aggregates dictates disaggregation. (A) Correlation between the extent of disaggregation ($\theta_{4\,\mu M}^{app}$) and the stability of the final soluble complex (K_d^{app}). Values are from Table 5.3. The black line represents the regression fit (R^2=0.58). (B) Correlation between the extent of disaggregation ($\theta_{4\,\mu M}^{app}$) and the stability of the starting aggregate (U_{50}) and the final soluble complex (K_d^{app}). Values are from Table 5.3. The black line represents the regression fit (R^2=0.77). Outliers highlighted in blue (Lhcb5, Lhcb5-H160C and Lhcb5-L170C) were included in the analyses.

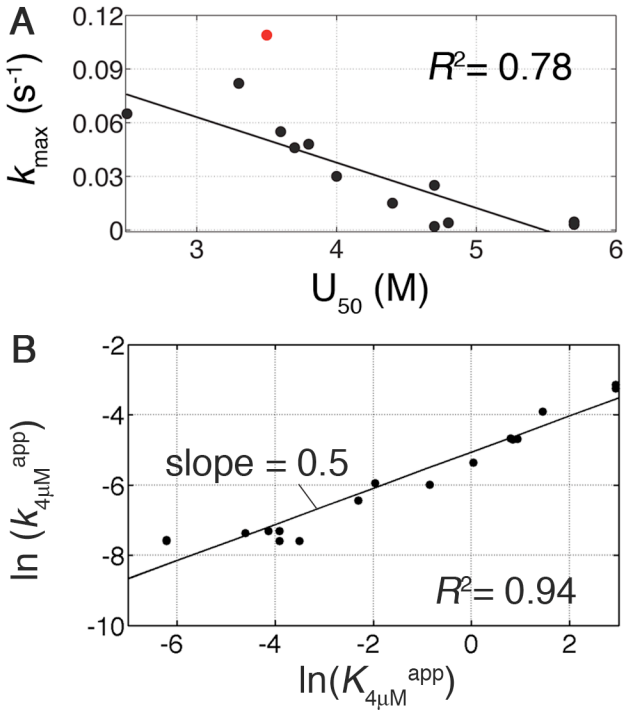

Figure 5.6 The rate and transition state analyses of LHCP disaggregation. (A) Correlation between U_{50} and the maximal rate of disaggregation (k_{max}). Values are from Table 5.3. The black line represents the regression fit (R^2=0.78). The red data point was excluded from the linear regression. (B) The Φ-analysis of LHCP disaggregation. The values of $K_{4\mu M}^{app}$ are calculated from $\theta_{4\mu M}^{app}$ values. The $k_{4\mu M}^{app}$ values are calculated from fits to eq 4. The black line represents a linear fit (R^2=0.94) with a slope of 0.5.

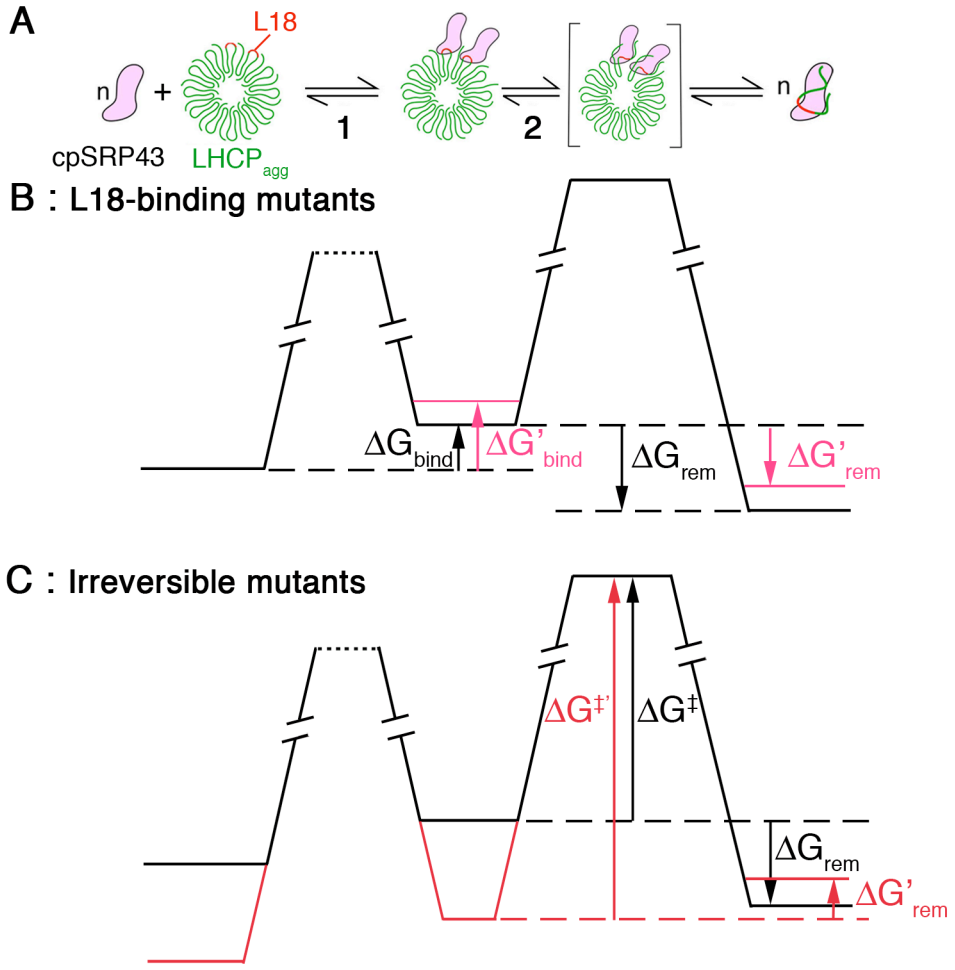

Figure 5.7 (A) Working model for cpSRP43-mediated disaggregation. Step 1 depicts initial binding of cpSRP43 (magenta) to the LHCP aggregate (green) via the solvent-exposed L18 motif (red). Step 2 depicts subsequent remodeling and re-solubilization of the LHCP aggregate. Two molecules of cpSRP43 are depicted for simplicity. These cpSRP43 molecules cooperatively disrupt the aggregate packing and lead to complete solubilization. (B) and (C) Qualitative free-energy diagrams summarizing the effects of the mutants that disrupt each step. The L18-binding mutants (B) primarily disrupt the initial binding step. Due to its defect in binding to the aggregate via compromised L18 affinity, the free energy cost to proceed to the intermediate cpSRP43•$LHCP_{agg}$ complex (ΔG_{bind}) is enlarged compared to wildtype (magenta vs. black). However, this defect can be overcome by high concentration of cpSRP43 to drive binding. The irreversible mutants (C) mostly affect the remodeling step by creating a deep well at the intermediate step due to the high stability of their aggregates. This results in both a larger activation barrier for remodeling ($\Delta G^{‡}$, red vs. black) and a thermodynamically unfavorable reaction (ΔG_{rem}, red vs. black). The figures are not drawn to scale.

Supplementary Table 1 Description of the LHCP TM mutants

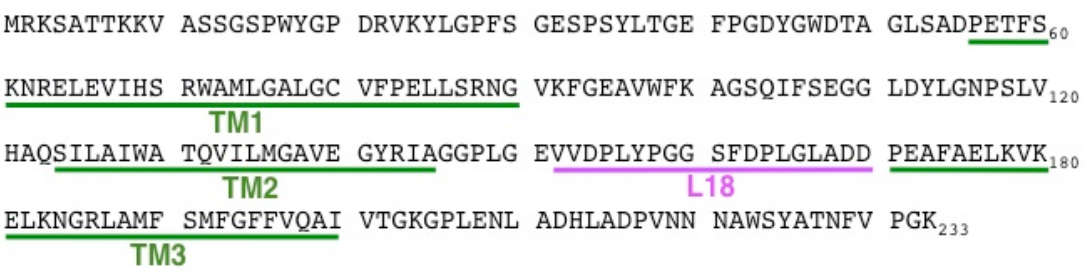

Construct	LHCP TM Replaced	Replaced by TM from	Amino acid sequence
WT	n/a	n/a	–
ΔTM1	TM1	–	–
ΔTM2	TM2	–	–
ΔTM3	TM3	–	–
1-1-3	TM2	LHCP TM1	PETFSKNRELEVIHSRWAMLGALGCVFPELLSRNG
1-3-3	TM2	LHCP TM3	PEAFAELKVKELKNGRLAMFSMFGFFVQAI
SERP2	TM2	SERP1	ASVGPWLLALFIFVVCGSAIF
Sec2	TM2	Sec61β	VPVLVMSLLFIASVFM
Cyb2	TM2	Cytochrome b5	NSSWWTNWVIPAISALIVALMY
1-2-1	TM3	LHCP TM1	PETFSKNRELEVIHSRWAMLGALGCVFPELLSRNG
1-2-2	TM3	LHCP TM2	SILAIWATQVILMGAVEGYRIA
SERP3	TM3	SERP1	ASVGPWLLALFIFVVCGSAIF
1-3-2	TM2, TM3	LHCP TM3, LHCP TM2	PEAFAELKVKELKNGRLAMFSMFGFFVQAI SILAIWATQVILMGAVEGYRIA

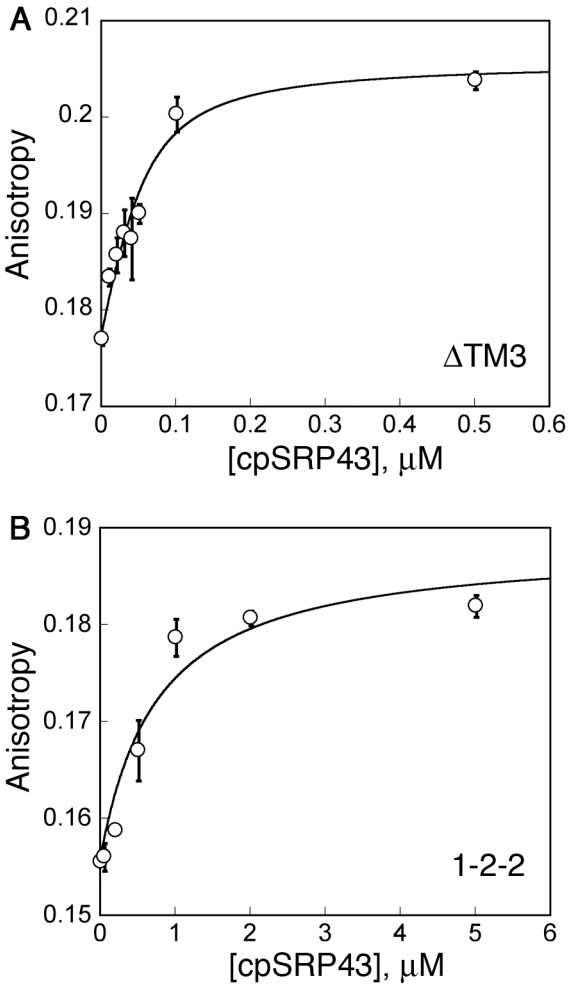

Supplementary Figure 5.S1 The binding affinities from light scattering are comparable to those from fluorescent anisotropy. Binding of ΔTM3 (A) and 1-2-2 (B) as measured by fluorescence anisotropy. The data were fit to a quadratic equation and gave K_d values of 22 nM for ΔTM3 and 713 nM for 1-2-2. For comparison, the K_d^{app} values measured by light scattering were 26 nM and 489 nM, respectively (Table 5.3).

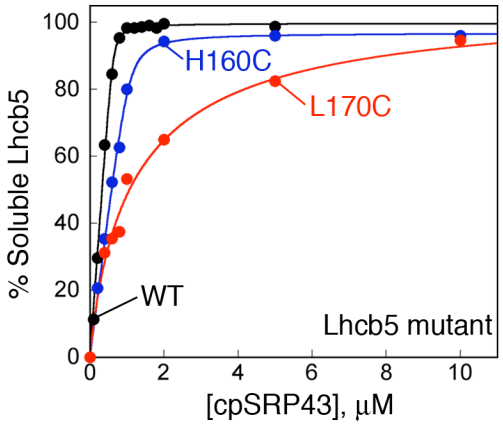

Supplementary Figure 5.S2 Binding of cpSRP43 to Lhcb5 and its L18 mutants as measured by light scattering. The data were fit to eq 1 and gave K_d^{app} values of 10 nM for Lhcb5 (black), 30 nM for Lhcb5-H160C (blue), and 1.1 μM for Lhcb5-L160C (red). The values are reported in Table 5.2.

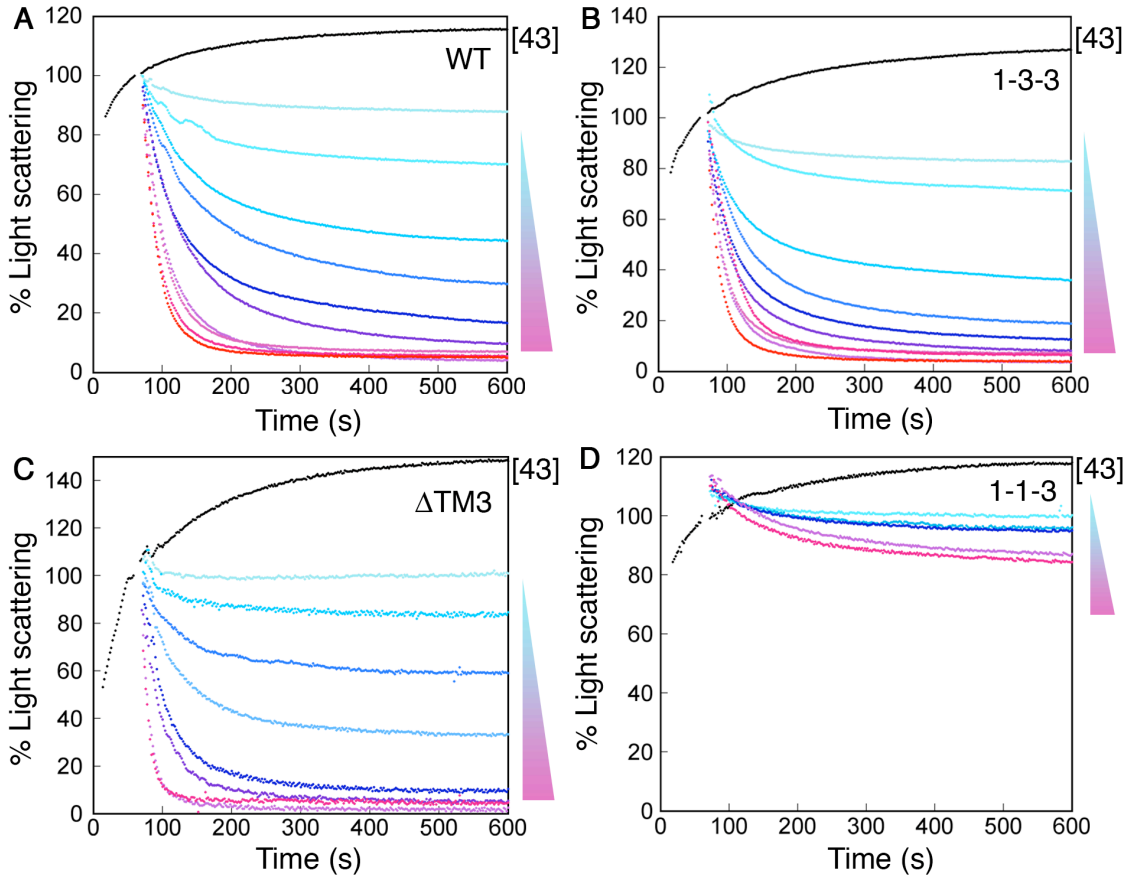

Supplementary Figure 5.S3 Disaggregation time courses with varying concentrations of cpSRP43 for LHCP WT (1–15 μM), 1-3-3 (1–15 μM), ΔTM3 (0.5–7 μM), and 1-1-3 (10–60 μM). These curves are representative of time courses derived from the disaggregation reactions of other LHCP TM mutants.

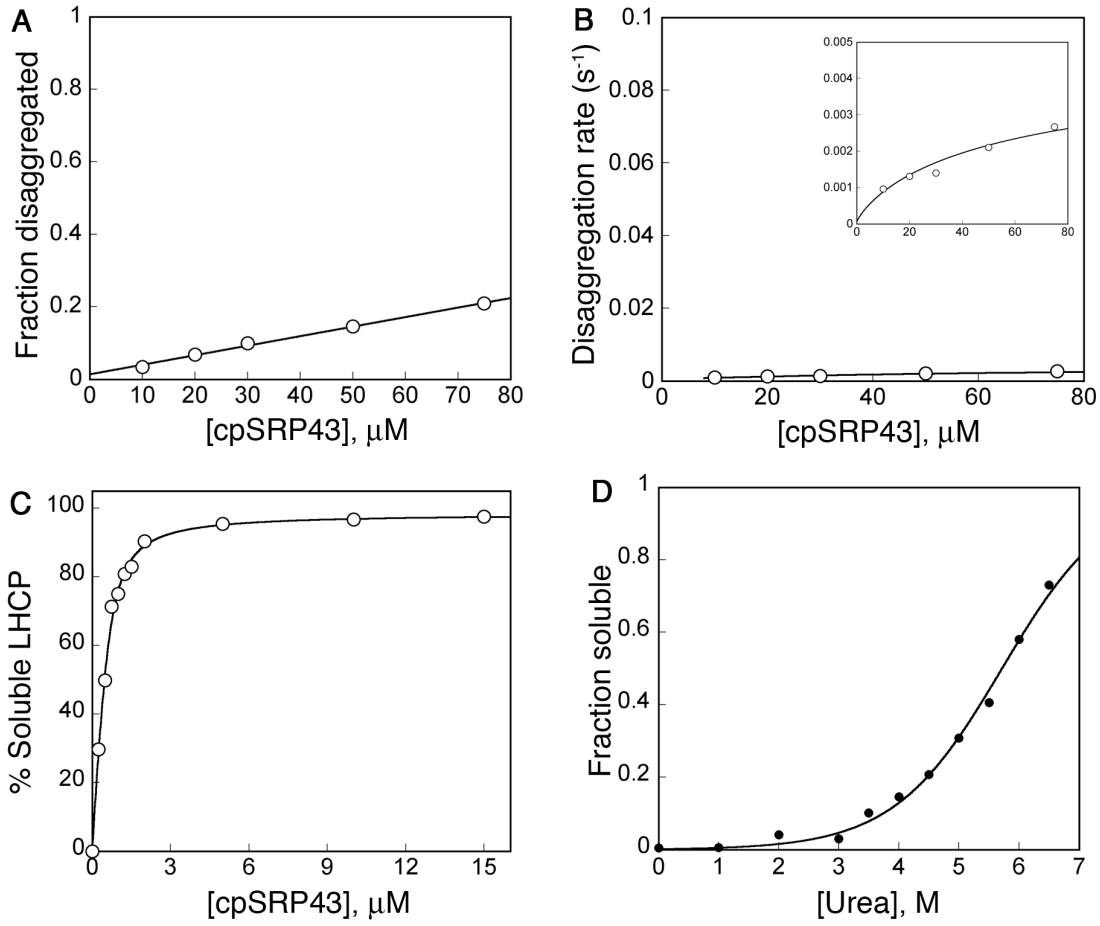

Supplementary Figure 5.S4 Thermodynamic and kinetic analyses for ΔTM2. (A) and (B) Concentration dependence of disaggregation equilibrium (A) and rate (B). (C) Binding of cpSRP43 to ΔTM2. (D) Urea solubilization curve for ΔTM2.

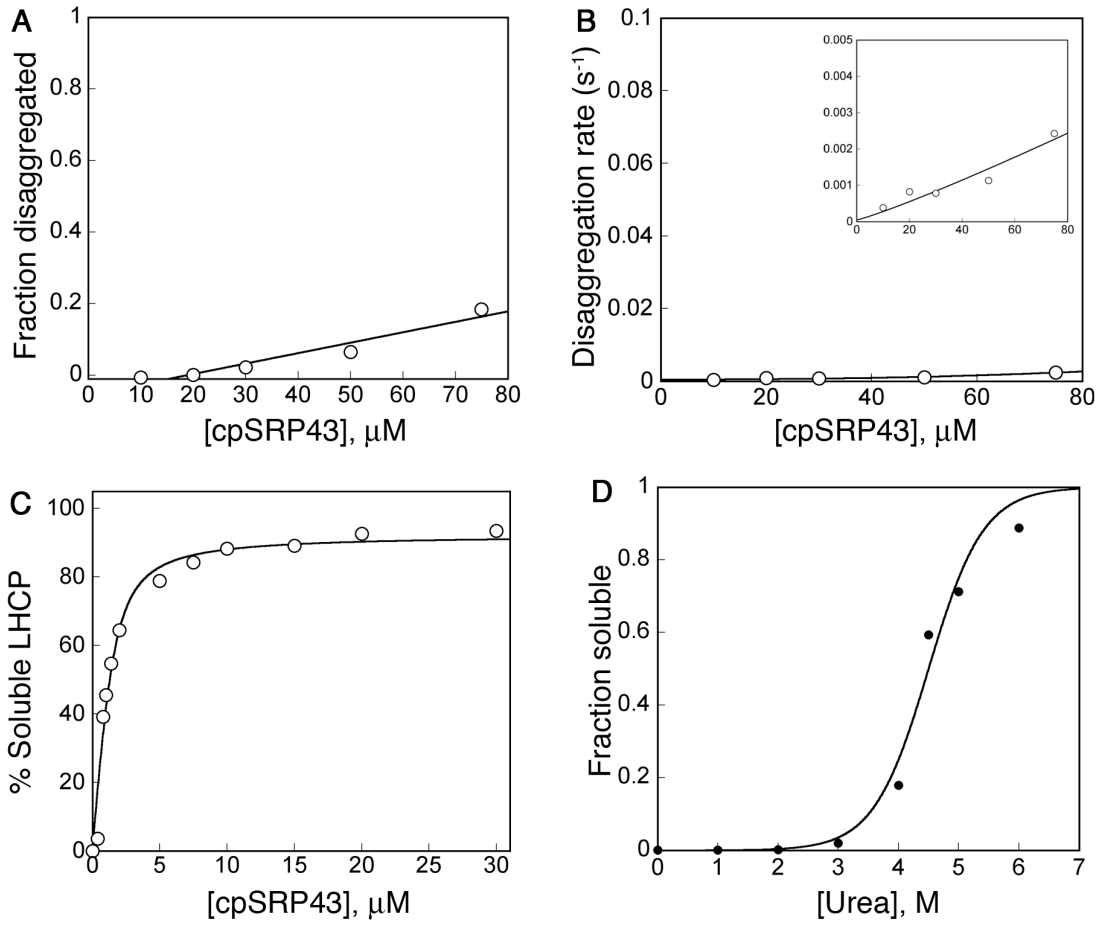

Supplementary Figure 5.S5 Thermodynamic and kinetic analyses for 1-2-2. (A) and (B) Concentration dependence of disaggregation equilibrium (A) and rate (B). (C) Binding of cpSRP43 to 1-2-2. (D) Urea solubilization curve for 1-2-2.

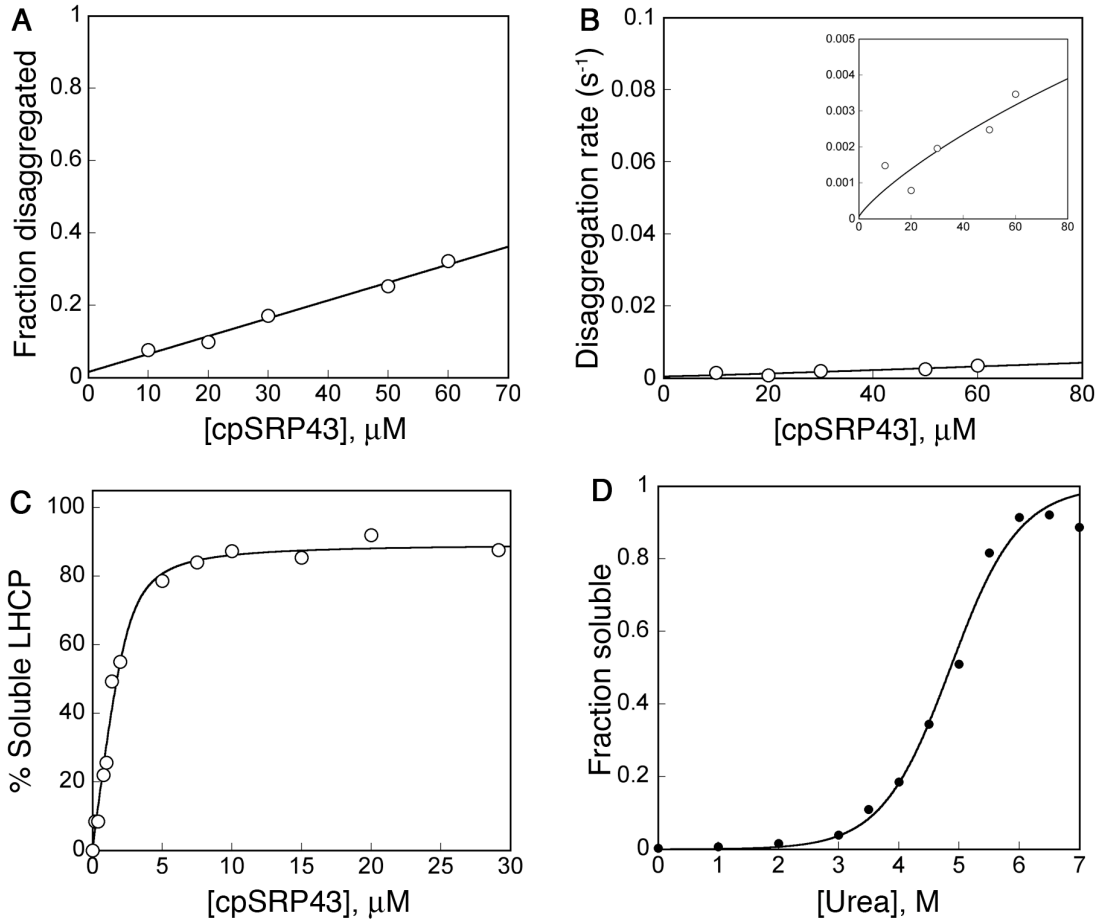

Supplementary Figure 5.S6 Thermodynamic and kinetic analyses for 1-3-2. (A) and (B) Concentration dependence of disaggregation equilibrium (A) and rate (B). (C) Binding of cpSRP43 to 1-3-2. (D) Urea solubilization curve for 1-3-2.

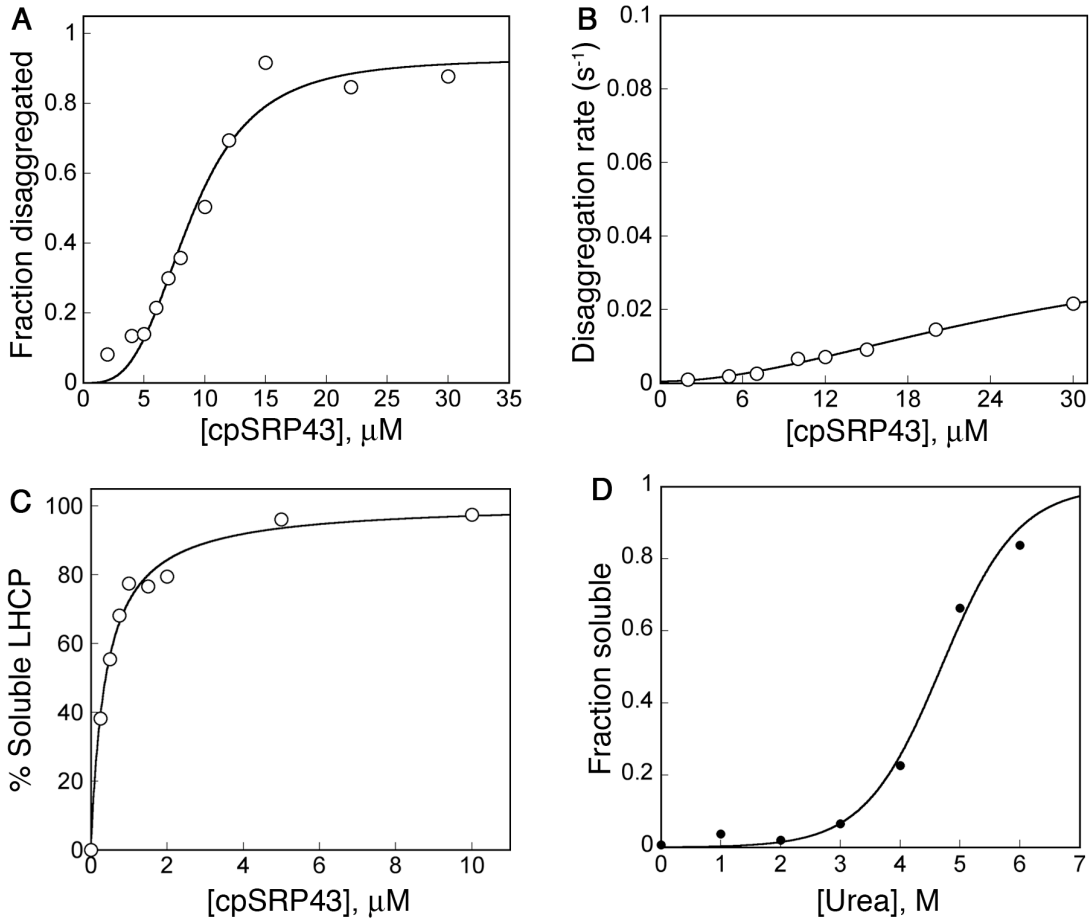

Supplementary Figure 5.S7 Thermodynamic and kinetic analyses for ΔTM1. (A) and (B) Concentration dependence of disaggregation equilibrium (A) and rate (B). (C) Binding of cpSRP43 to ΔTM1. (D) Urea solubilization curve for ΔTM1.

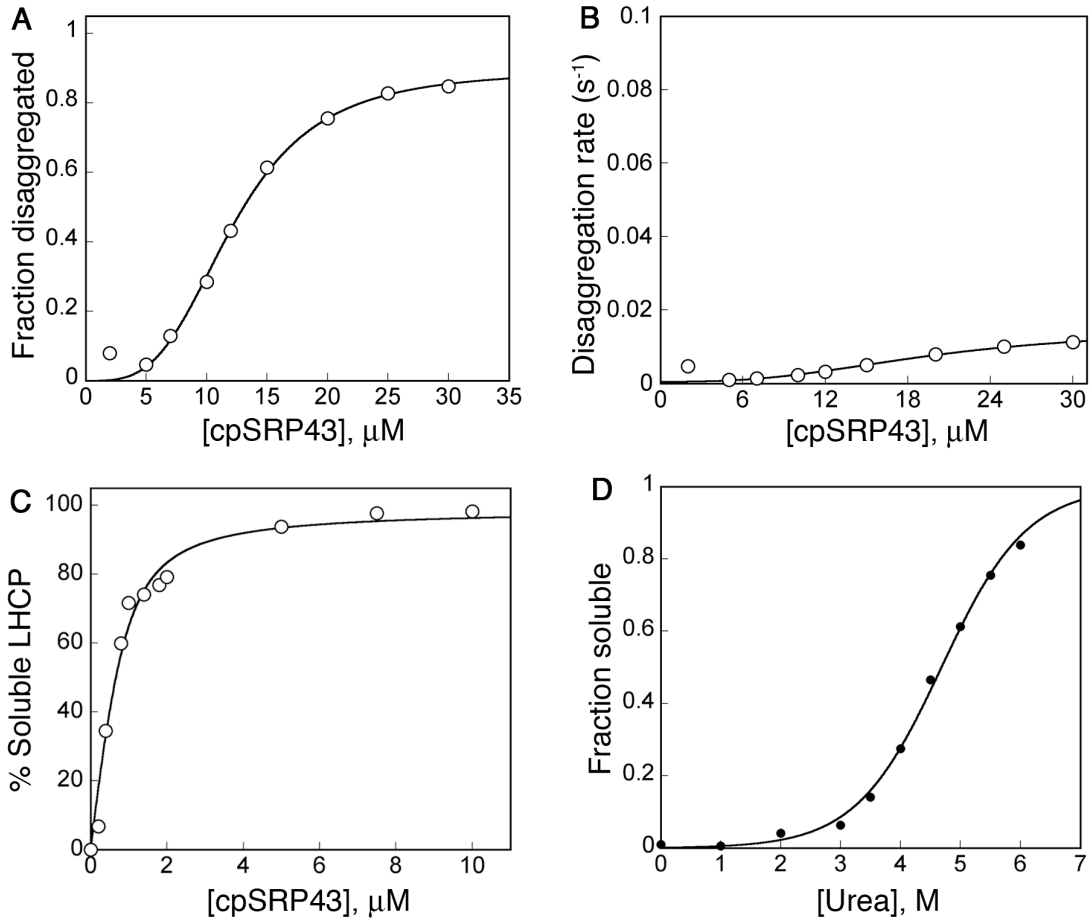

Supplementary Figure 5.S8 Thermodynamic and kinetic analyses for 1-2-1. (A) and (B) Concentration dependence of disaggregation equilibrium (A) and rate (B). (C) Binding of cpSRP43 to 1-2-1. (D) Urea solubilization curve for 1-2-1.

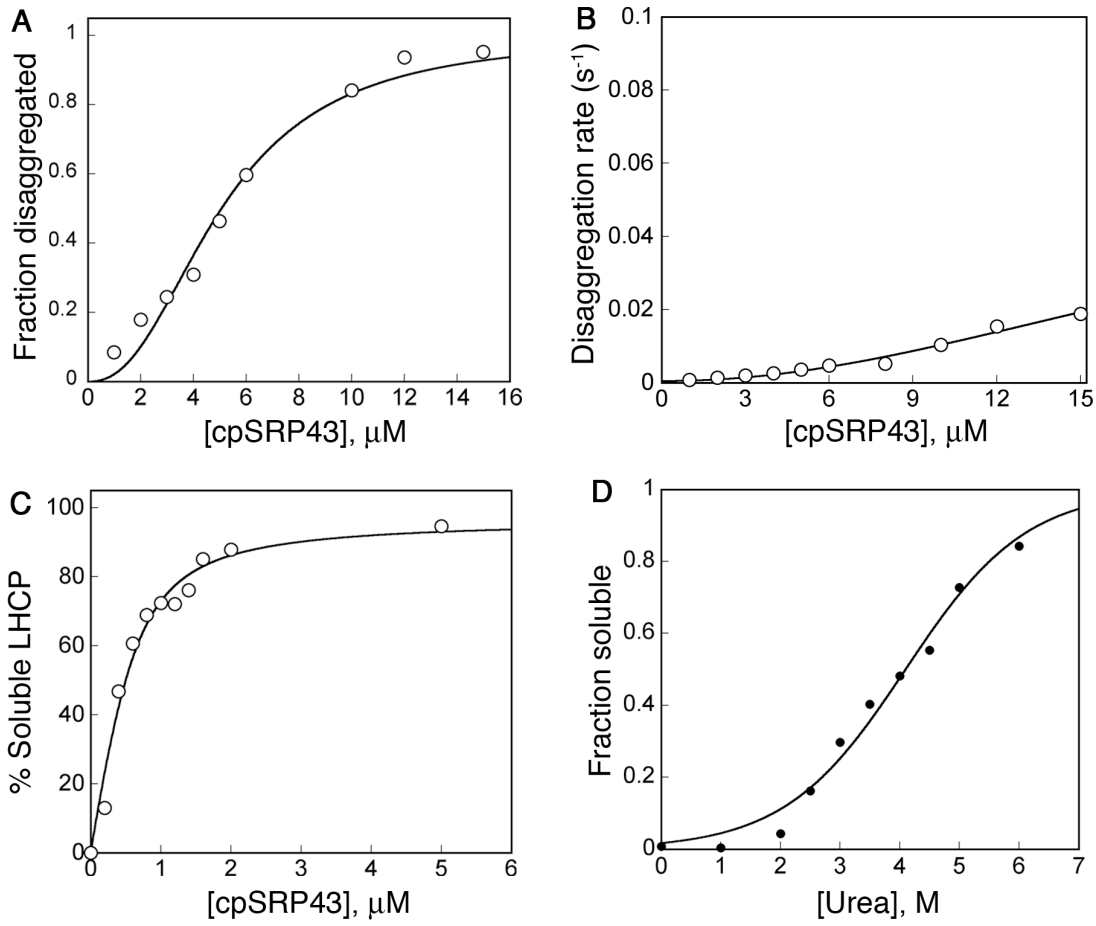

Supplementary Figure 5.S9 Thermodynamic and kinetic analyses for SERP3. (A) and (B) Concentration dependence of disaggregation equilibrium (A) and rate (B). (C) Binding of cpSRP43 to SERP3. (D) Urea solubilization curve for SERP3.

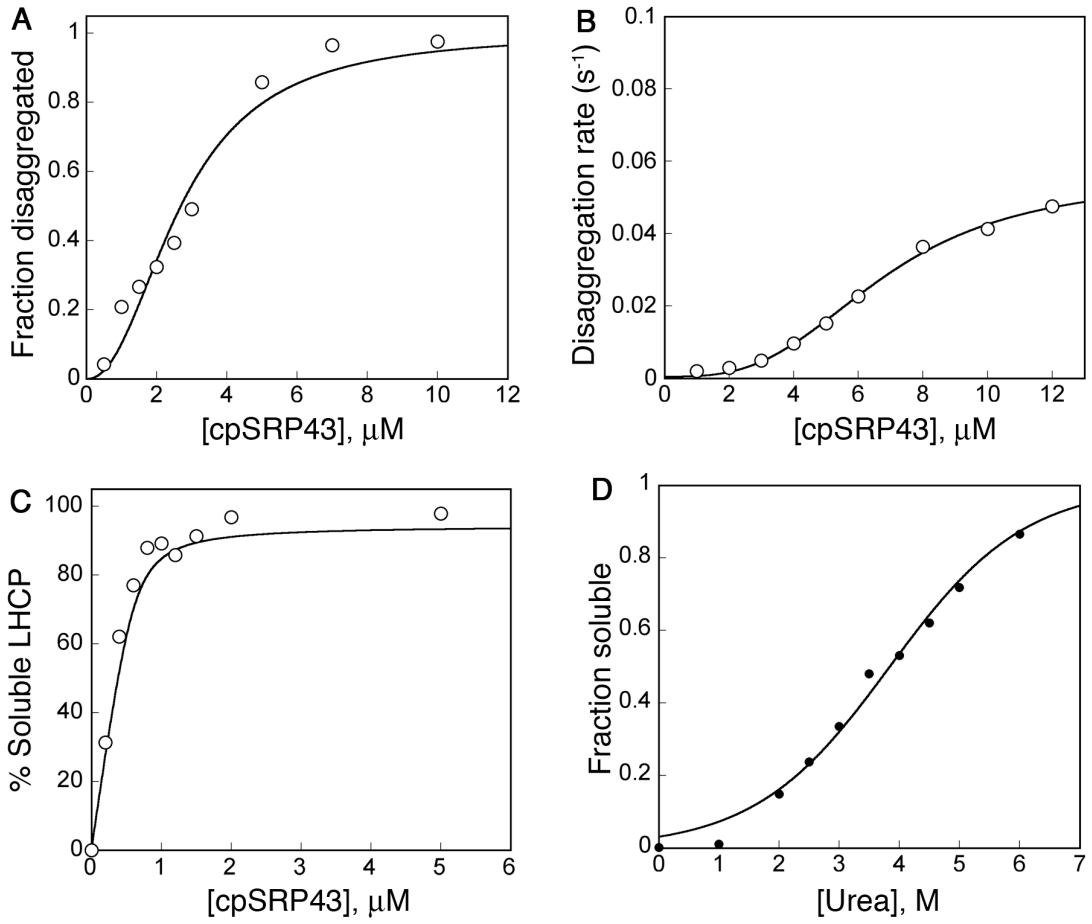

Supplementary Figure 5.S10 Thermodynamic and kinetic analyses for Cyb2. (A) and (B) Concentration dependence of disaggregation equilibrium (A) and rate (B and inset). (C) Binding of cpSRP43 to Cyb2. (D) Urea solubilization curve for Cyb2.

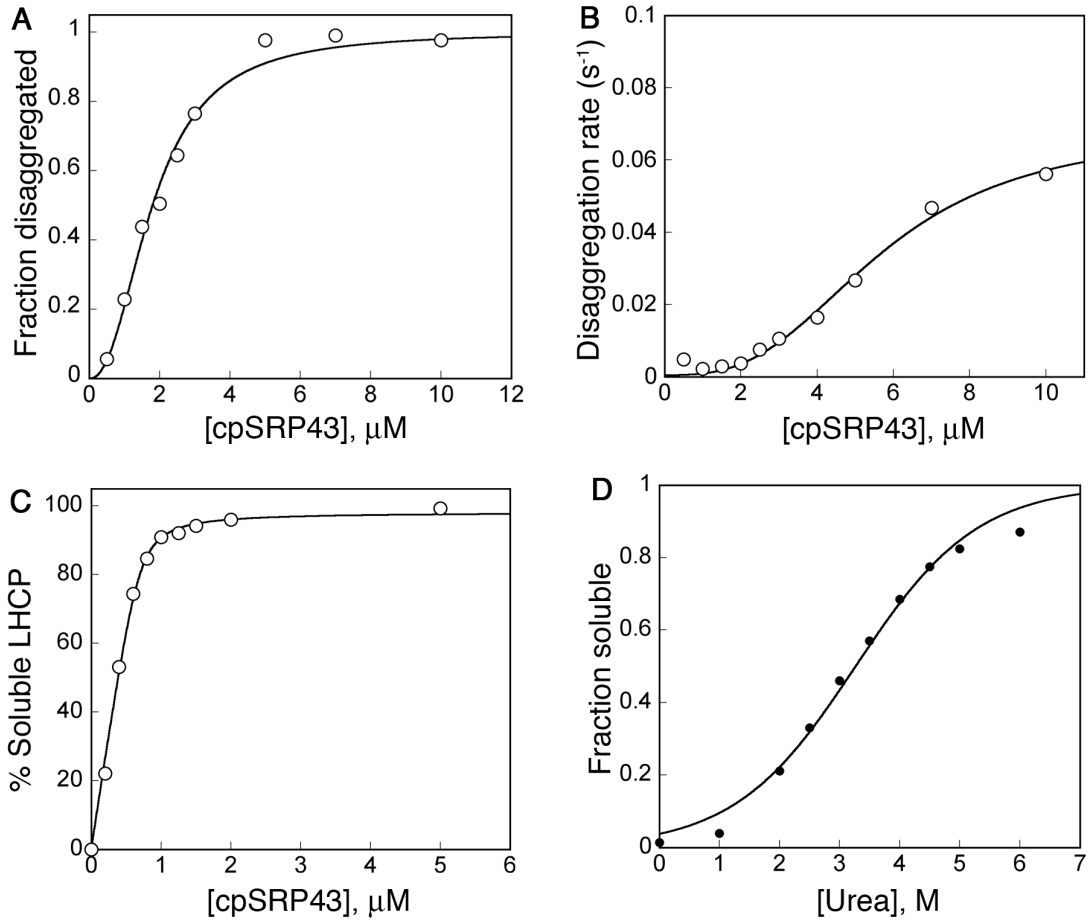

Supplementary Figure 5.S11 Thermodynamic and kinetic analyses for Sec2. (A) and (B) Concentration dependence of disaggregation equilibrium (A) and rate (B and inset). (C) Binding of cpSRP43 to Sec2. (D) Urea solubilization curve for Sec2.

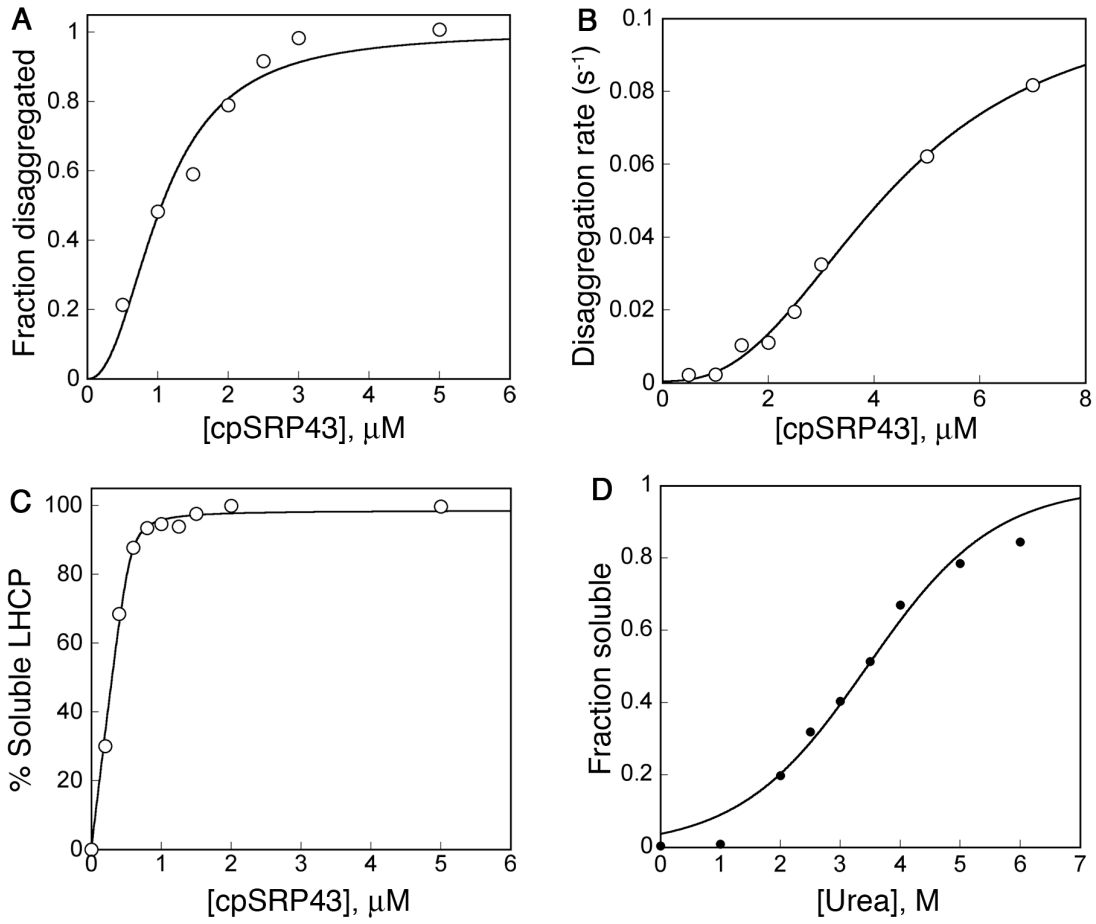

Supplementary Figure 5.S12 Thermodynamic and kinetic analyses for SERP2. (A) and (B) Concentration dependence of disaggregation equilibrium (A) and rate (B and inset). (C) Binding of cpSRP43 to SERP2. (D) Urea solubilization curve for SERP2.

References:

1. Balch, W. E., Morimoto, R.I., Dillin, A., and Kelly, J.F. (2008) Adapting proteostasis for disease intervention, *Science 319*, 916–919.
2. Hayer-Hartl, M., and Hartl, F.U. (2002) Molecular chaperones in the cytosol: from nascent chain to folded protein, *Science 295*, 1852–1858.
3. Chang, H.-C., Tang, Y.-C., Hayer-Hartl, M., and Hartl, F.U. (2007) Snapshot: Molecular chaperones, part I, *Cell 128*, 212–213.
4. Tang, Y.-C., Chang, H.-C., Hayer-Hartl, M., and Hartl, F.U. (2007) Snapshot: Molecular chaperones, part II, *Cell 128*, 412–413.
5. Doyle, S. M., and Wickner, S. (2008) Hsp104 and ClpB: protein disaggregating machines, *Trends Biochem. Sci. 34*, 40–48.
6. Haslberger, T., Bukau, B., and Mogk, A. (2010) Towards a unifying mechanism for ClpB/Hsp104-mediated protein disaggregation and prion propagation, *Biochem. Cell Biol. 88*, 63–75.
7. Glover, J. R., and Lindquist, S. (1998) Hsp104, Hsp70, and Hsp40: a novel chaperone system that rescues previously aggregated proteins, *Cell 94*, 73–82.
8. Goloubinoff, P., Mogk, A., Ben Zvi, A.P., Tomoyasu, T., and Bukau, B. (1999) Sequential mechanism of solubilization and refolding of stable protein aggregates by a bichaperone network, *Proc. Natl. Acad. Sci. USA 96*, 13732–12737.
9. Bieschke, J., Cohen, E., Murray, A.N., Dillin, A., and Kelly, J.W. (2009) A kinetic assessment of the *C. elegans* amyloid disaggregation activity enables uncoupling of disassembly and proteolysis, *Protein Science 18*, 2231–2241.
10. Murray, A. N., Solomon, J.P., Wang, Y-J., Balch, W.E., and Kelly, J.W. (2010) Discovery and characterization of a mammalian amyloid disaggregation activity, *Protein Science 19*, 836–846.
11. Jaru-Ampornpan, P., Shen, K., Lam, V.Q., Ali, M., Doniach, S., Jia, T.Z., and Shan, S. (2010) ATP-independent reversal of a membrane protein aggregate by a chloroplast SRP subunit, *Nat. Struct. Mol. Biol. 17*, 696–702.
12. Schuenemann, D., Gupta, S., Persello-Cartieaux, F., Klimyuk, V. I., Jones, J. D. G., Nussaume, L., and Hoffman, N. E. (1998) A novel signal recognition particle targets light-harvesting proteins to the thylakoid membranes, *Proc. Natl. Acad. Sci. USA 95*, 10312–10316.
13. Jansson, S. (1999) A guide to the Lhc genes and their relatives in arabidopsis, *Trends Plant Sci. 4*, 236–240.
14. Liu, Z., Yan, H., Wang, K., Kuang, T., Zhang, J., Gui, L., An, X., and Chang, W. (2004) Crystal structure of spinach major light-harvesting complex at 2.72 Å resolution, *Nature 428*, 287–292.
15. Tu, C. J., Peterson, E. C., Henry, R., and Hoffman, N. E. (2000) The L18 domain of light-harvesting chlorophyll proteins binds to chloroplast signal recognition particle 43, *J. Biol. Chem. 275*, 13187–13190.
16. Delille, J., Peterson, E. C., Johnson, T., Morre, M., Kight, A., and Henry, R. (2000) A novel precursor recognition element facilitates posttranslational binding to the signal recognition particle in chloroplasts, *Proc. Natl. Acad. Sci. 97*, 1926–1931.

17. Stengel, K. F., Holdermann, I., Cain, P., Robinson, C., Wild, K., and Sinning, I. (2008) Structural basis for specific substrate recognition by the chloroplast signal recognition particle protein cpSRP43, *Science 321*, 253–256.
18. Klimyuk, V. I., Persello-Cartieaux, F., Havaux, M., Contard-David, P., Schuenemann, D., Meiherhoff, K., Gouet, P., Jones, J.D.G., Hoffman, N.E., and Nussaume, L. (1999) A chromodomain protein encoded by the arabidopsis CAO gene is a plant-specific component of the chloroplast signal recognition partivle pathway that is involved in LHCP targeting, *The Plant Cell 11*, 87–99.
19. Eichacker, L. A., and Henry, R. (2001) Function of a chloroplast SRP in thylakoid protein export, *Biochim. Biophys. Acta 1541*, 120–134.
20. Jonas-Straube, E., Hutin, C., Hoffman, N.E., and Schuenemann D. (2001) Functional analysis of the protein-interacting domains of chloroplast SRP43, *J. Biol. Chem. 276*, 24654–24660.
21. Abramoff, M. D., Magelhaes, P.J., and Ram, S.J. (2004) Image Processing with ImageJ, *Biophotonics International 11*, 36–42.
22. Fersht, A. (1998) *Structure and mechanism in protein science: a guide to enzyme catalysis and protein folding*, W.H. Freeman and Company, New York.
23. D'Errico, J. (2006) Polyfitn, N-d polynomial regression model.
24. Cain, P., Holdermann, I., Sinning, I., Johnson, A.E., and Robinson, C. (2011) Binding of chloroplast signal recognition particle to a thylakoid membrane protein substrate in aqueous solution and delineation of the cpSRP43-substrate interaction domain, *Biochem J.* Epub ahead of print (April 5, 2011).
25. Mogk, A., Dougan, D., Weibezahn, J., Schlieker, C., Turgay, K., and Bukau, B. (2004) Broad yet high substrate specificity: the challenge of AAA+ proteins, *J. Struct. Biol. 146*, 90–98.
26. Schlieker, C., Weibezahn, J., Patzelt, H., Tessarz, P., Strub, C., Zeth, K., Erbse, A., Schneider-Mergener, J., Chin, J.W., Schultz, P.G., Bukau, B., and Mogk, A. (2004) Substrate recognition by the AAA+ chaperone ClpB, *Nat Struct Mol Biol. 11*, 607–615.
27. Weibezahn, J., Tessarz, P., Schlieker, C., Zahn, R., Maglica, Z., Lee, S., Zentgraf, H., Weber-Ban, E.U., Dougan, D.A., Tsai, F.T., Mogk, A., and Bukau, B. (2003) Thermotolerance requires refolding of aggregated proteins by substrate translocation through the central pore of ClpB, *Cell 119*, 653–665.
28. Lee, C., Schwartz, M.P., Prakash, S., Iwakura, M., and Matouschek, A. (2001) ATP-dependent proteases degrade their substrates by processively unraveling them from the degradation signal, *Mol Cell 7*, 627–637.
29. Kenniston, J. A., Baker, T.A., Fernandez, J.M., and Sauer, R.T. (2003) Linkage between ATP consumption and mechanical unfolding during the protein processing reactions of an AAA+ degradation machine, *Cell 114*, 511–520.
30. Kenniston, J. A., Burton, R.E., Siddiqui, S.M., Baker, T.A., and Sauer, R.T. (2004) Effects of local protein stability and the geometric position of the substrate degradation tag on the efficiency of ClpXP denaturation and degradation, *J Struct Biol 146*, 130–140.
31. Henry, R. L. (2010) SRP: Adapting to life in the chloroplast, *Nat Struct Mol Biol. 17*, 676–677.